ARMY RESEARCH LABORATORY

Self-Assembling Nanomembranes Through Electrostatic Melt Processing of Copolymer Films

by Eric D. Wetzel and Frederick L. Beyer

ARL-TR-2800 August 2002

NOTICES

Disclaimers

The findings in this report are not to be construed as an official Department of the Army position unless so designated by other authorized documents.

Citation of manufacturer's or trade names does not constitute an official endorsement or approval of the use thereof.

Destroy this report when it is no longer needed. Do not return it to the originator.

Army Research Laboratory
Aberdeen Proving Ground, MD 21005-5069

ARL-TR-2800 **August 2002**

Self-Assembling Nanomembranes Through Electrostatic Melt Processing of Copolymer Films

Eric D. Wetzel and Frederick L. Beyer
Weapons and Materials Research Directorate, ARL

Abstract

Polystyrene-polyisobutylene-polystyrene (SIBS) block copolymer films have been electrostatically melt processed in order to induce a preferential orientation in the material microstructure. The results show that electrostatic melt processing is inducing some change in the microstructure, but full reorientation is not being achieved. The low dielectric contrast of the SIBS blocks as well as the relatively short electrostatic processing times are the likely causes of incomplete alignment.

Acknowledgments

The authors would like to acknowledge Prof. Sam Gido and Yuqing Zhu at the University of Massachusetts Amherst for their assistance in preparing and imaging the transmission electron microscopy samples.

INTENTIONALLY LEFT BLANK.

Contents

INTENTIONALLY LEFT BLANK.

List of Figures

INTENTIONALLY LEFT BLANK.

1. Introduction

1.1 Selective Membranes for U.S. Army Applications

A selective membrane is a barrier layer which is designed to allow efficient transport of only particular fluids, vapors, particulates, or chemicals. Advanced selective membrane materials could provide significant advances in the capabilities of Army forces. Two applications of specific interest are chem-bio suits and fuel cell membranes.

Chem-bio suits must prevent transport of any hazardous chemical or biological agent. Currently fielded chem-bio suits are fabricated from butyl rubber or polyisobutylene films. These materials effectively prevent transport of nearly any physical or chemical species, providing excellent chem-bio protection. A serious limitation of these materials, however, is that they also prevent the transport of water. When a soldier wearing the suit perspires, the perspiration is not able to freely evaporate into the surroundings. As a result, the soldier quickly becomes very hot and uncomfortable, limiting soldier stamina and performance. The discomfort of these suits often prompts soldiers to choose not to wear the suits at all, even in threatening situations, making them highly vulnerable to chem-bio attack.

A selective membrane material could provide significant advantages over conventional materials for chem-bio suit fabrics. This superior barrier material would allow the transport of water through its thickness, while still completely blocking harmful chem-bio agents. Such a material would allow fabrication of chem-bio suits which would be both protective and comfortable, greatly enhancing the capabilities of the soldier.

Fuel cells produce electricity through the steady, low-temperature oxidation of a hydrocarbon fuel. Compared with conventional power sources such as batteries and internal combustion engines, fuel cells are quieter, have a higher energy density, and are scalable over a range of sizes. These advantages make fuel cells well suited to soldier personal power generation and stealthy vehicles.

A critical component in fuel cells is the proton exchange membrane. Maximum fuel cell power and longevity are achieved if this membrane material prevents transport of all species except for hydrogen ions. In most cases, materials which transport hydrogen ions efficiently also transport water molecules efficiently. Therefore, both fuel cells and chem-bio suits could benefit from the development of new membrane materials which allow for selective, efficient transport of water. The demands of Army applications impose that these materials also offer rugged mechanical properties, easy processibility, and relatively low cost.

1.2 Polystyrene-Polyisobutylene-Polystyrene (SIBS) Block Copolymers

One promising selective membrane material which has been identified is SIBS triblock copolymer. Due to repulsive enthalpic interactions between its homopolymer blocks, this material phase separates into a two-phase structure. The particular structure which evolves is determined by the molecular weights of the blocks and processing.

Previous studies have shown that water transport through SIBS films can be enabled by sulfonating the polystyrene phase [1, 2]. The particular grade of SIBS used in these studies formed a structure comprised of cylinders of polysterene (PS) in a matrix of polyisobutylene (PIB). The cylinders had a diameter of ~50 nm and, when cast from dilute solution, formed films in which the cylinders were aligned in the plane of the film.

Since the PS phase is responsible for water transport in the sulfonated SIBS film, it is reasonable to expect that the efficiency of water transport could be enhanced by alignment of the cylindrical PS domains in the preferred transport direction. Unfortunately, thermodynamic driving forces during processing tend to strongly orient the PS phase in the film plane, limiting the thru-thickness transport. Therefore, it would be advantageous to develop a means of processing SIBS films such that the cylindrical PS domains are oriented normal to the film plane.

1.3 Electric Field-Induced Orientation in Block Copolymers

Previous researchers have shown that electric fields can be used to preferentially reorient microstructures in block copolymer films [3–9]. The reorientation is driven by electrostatic forces, which cause anisotropic dielectric structures to align with the electric field direction. The rate at which this reorientation occurs depends on the state of the material during application of the electric field. There are three main reorientation mechanisms—domain dissolution, domain flow, and domain rotation. These mechanisms are illustrated schematically in Figure 1.

For illustration, we will consider the microstructure of a dielectric ellipsoidal phase immersed in a matrix of a different dielectric phase. Domain reorientation is only possible if the matrix phase of the block copolymer is the melt state. If the ellipsoidal phase is solid, then rotation occurs through solid body rotation through the matrix fluid [10, 11]. This process has been shown to reorient short glass and ceramic fibers in a dielectric fluid [12, 13]. If the ellipsoidal phase is a liquid, then reorientation can occur through deformation and flow of the ellipsoidal phase [14, 15]. This process is, in general, faster that the solid rotation process due to the high hydrodynamic resistance associated with solid body rotation in a fluid. This difference is made even more acute as the aspect ratio of the ellipsoidal phase is increased. The domain flow reorientation mechanism has been demonstrated in block copolymers in only a few cases [9] due to the advantages of the domain dissolution method.

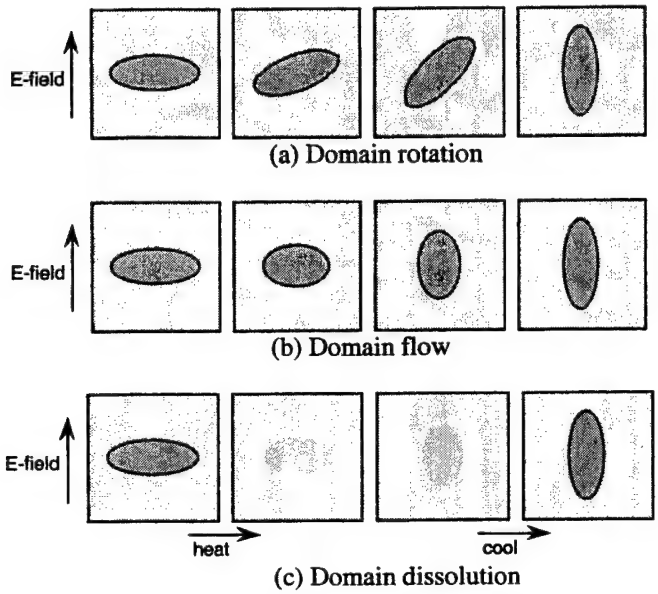

Figure 1. Electrostatic microstructural alignment mechanisms in block copolymers.

Domain dissolution requires a block copolymer system whose homopolymers become miscible above a characteristic temperature called the order-disorder temperature (ODT). Above the ODT, the two-phase structure is replaced by an amorphous structure. Upon cooling through the ODT, the amorphous structure reverts to the two-phase structure. If an electric field is applied during this cooling process, the two-phase structure forms with a preferential orientation in the electric field direction [4–9]. The kinetics of this alignment process are generally faster than the rotation or flow mechanisms. For this reason, nearly all of the successfully oriented block copolymers have been electrostatically processed using this dissolution mechanism.

Researchers have estimated that the ODT of SIBS is greater than 300 °C [16], which is well above the thermal degradation limits of the material. Therefore, the domain dissolution mechanism is not applicable to this material. The glass transition temperature (T_g) of PIB (an elastomer) is -70 °C, while the T_g of PS is ~95 °C. Therefore, by electrostatic melt processing SIBS well above 95 °C, a domain flow realignment mechanism is possible.

The dielectric constant of PS is 2.5, while the dielectric constant of PIB is 2.2. The resulting ratio of dielectric constants is 1.14. This dielectric contrast is small, which results in a relatively low electrostatic alignment driving force. As a comparison, Amundson et al. [9] demonstrated electrostatic orientation via domain flow for a PS-polymethylmethacrylate (PMMA) diblock copolymer. The dielectric constant of PMMA is 3.6, providing a dielectric ratio in PS-PMMA of 1.44. (It should be noted that these values for dielectric constant are based on room temperature measurements. The dielectric constants of many polymers

change drastically with temperature, so the actual dielectric contrast at processing temperatures may be very different from these room temperature estimations.)

1.4 Objective

The objective of this study is to demonstrate the use of electrostatic melt processing to create thick SIBS films in which the cylindrical PS phases are oriented normal to the film plane. The use of SIBS film is unique to this work and has two important implications. First, the relatively low dielectric contrast of the phases, as well as the limitations of the domain flow mechanism, will make electrostatic alignment very challenging. Second, if alignment in SIBS films is achieved, it will open the possibility for enhanced film transport properties. The use of electrostatic melt processing for modification of material transport properties is a unique application of this processing approach.

2. Experimental

2.1 Electrostatic Melt-Processing Apparatus

Figure 2 shows the electrostatic melt-processing apparatus used in this investigation. The SIBS sample is sandwiched between electrodes which are attached to a high-voltage power supply. The electrode-SIBS-electrode sandwich is placed on top of a resistive strip heater, which heats the SIBS film via direct conduction. The process control thermocouple is located on top of the stack to provide a conservative estimate of the film temperature. A programmable controller is used to control the thermal history of the sample, while the applied voltage is set manually. The entire stack is thermally and electrically insulated from the surroundings. The total stack thickness, from the top of the strip heater to the bottom of the thermocouple, is ~3 mm.

Figure 3 shows the electrode and sample geometry in the poling stack. The SIBS film is placed within a 6-mm × 6-mm window of 75-μm-thick Kapton (a registered trademark of DuPont) film. The Kapton window limits flow of the molten SIBS and provides some degree of film thickness control. Typically, 5-mm × 5-mm × 100-μm-thick samples of SIBS film are processed. The electrodes are fabricated from 25-μm-thick aluminized Kapton film, with the Kapton side facing the SIBS film.

2.2 Materials

The SIBS used in this study was obtained from Kuraray Company, Ltd., Japan. This triblock copolymer has a PS content of 30 weight-percent, with an average molecular weight of 72,000 g/mol and a polydispersity index of 1.47. The

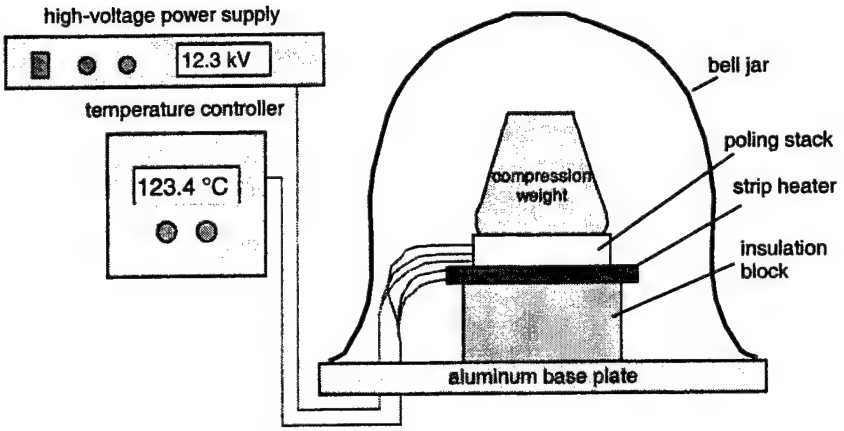

(a) General view

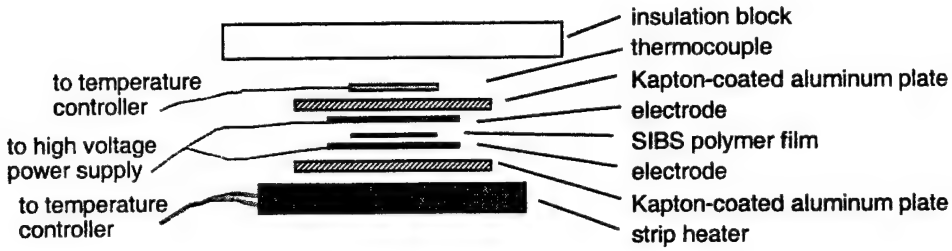

(b) Expanded view of poling stack

Figure 2. Schematic of the electrostatic melt-processing apparatus.

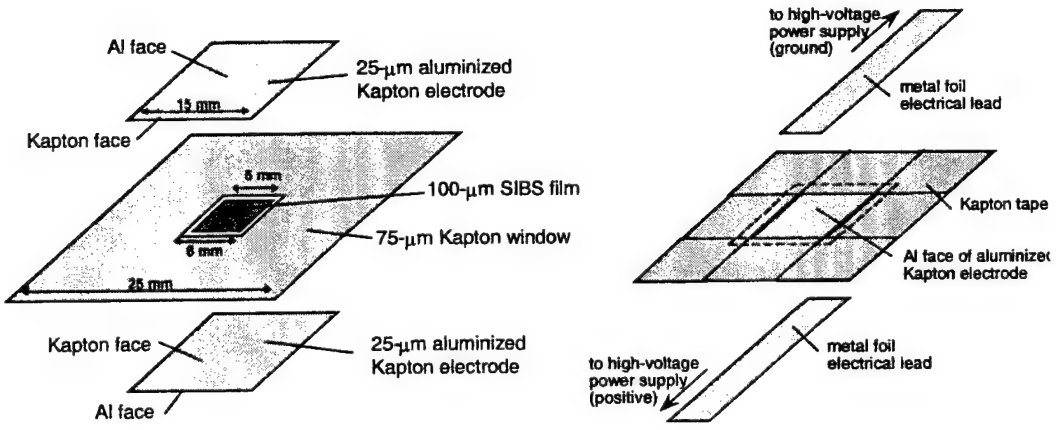

Figure 3. Close-up of the poling stack of the electrostatic melt-processing apparatus.

original pellets were melt processed in a hot press to create the 100-μm-thick film used for electrostatic melt processing.

2.3 Processing

Because the domain flow mechanism is expected to be relatively slow, it is advantageous to select processing conditions which maximize the rate of orientation. The rate of flow is increased as the phase viscosities decrease. Therefore, the rate of orientation will be fastest at higher temperatures. However, if the processing temperature is too high, thermal degradation will damage the material. We chose to use a processing temperature of 250 °C, a reasonably high temperature at which the rate of thermal degradation is relatively slow.

The rate of flow reorientation should also increase as the electric field strength increases. For a given electrode spacing, the electric field strength increases linearly with voltage. The applied electric field cannot exceed the dielectric field strength of any of the materials in the electrode stack. We found that the Kapton film used for both the sample window and the electrodes exhibited dielectric breakdown at an electric field strength of ~100 kV/mm at 250 °C (the dielectric strength of Kapton film is at least 50% higher at room temperature). During processing, flow of the SIBS material would sometimes create areas where the Kapton faces of the electrodes would be in direct contact. Since each Kapton layer was 25 μm in thickness, dielectric breakdown would occur if the applied voltage exceeded 5 kV. In practice, it was necessary to limit the applied voltage to 3 kV. Since the electrodes were spaced by two 25-μm-thick pieces of Kapton and a 100-μm-thick film of SIBS, the applied electric field strength across the SIBS film was 20 kV/mm at 3 kV.

Increased time in the electrostatic field at elevated temperatures should also improve the degree of reorientation. In practice, 1 hr was the maximum elevated temperature processing time that could be implemented with reasonable consistency. Longer process times frequently led to electrical shorts or component dielectric breakdown, which eliminated the electric field across the SIBS film thickness.

Two different processing runs were performed. In both cases, the sample was heated from room temperature to 250 °C over 30 min, held at 250 °C for 1 hr, and then cooled to room temperature. The cooling rate was not controlled (the heater power was simply turned off after dwell), but the total cooling time was ~1 hr. For the first case, this thermal processing was performed without an applied electric field. In the second case, a voltage of 3 kV (corresponding to an electric field strength of 20 kV/mm) was applied during the entire heating, dwell, and cooling process. As a comparison, microstructural characterization was also performed on film which was neither thermally or electrostatically processed.

These three samples should allow comparison of microstructures for unprocessed, heat-only, and heat with electric field conditions.

2.4 Characterization

2.4.1 Small-Angle X-ray Scattering (SAXS)

The characterization of the morphology in the films was done primarily by small-angle x-ray scattering (SAXS). A Rigaku Ultrax 3-kW rotating anode x-ray generator, operated at 40 kV, 60 mA, and with a Cu anode, was the source of the radiation. A pyrolytic graphite monochromator was used to filter out characteristic Cu-K_β radiation, leaving only the Cu-K_α doublet with an average wavelength of $\lambda = 1.5418$ Å. The SAXS camera is an Anton-Paar HR-PHK single-pinhole design, which uses one pinhole 100 μm in diameter 6 cm upstream of the sample to collimate the x-ray beam. A 300-μm scatter shield is located 2 cm upstream of the sample and eliminates parasitic scattering. The data is collected using a Bruker Hi-Star area detector and GADDS software. Circularly averaged intensity is presented as a function of the magnitude of the scattering vector, q ($Å^{-1}$), where q is defined by $q = 4\pi \cdot \sin(\theta)/\lambda$.

Previously, the maximum length scale for any SAXS feature that could be clearly determined by the unmodified Anton-Paar camera was ~25 nm. This resolution limitation was due to the camera design, which relied upon the emission of x-rays from the rotating anode source having a specific geometry. In that case, the rotating anode source acted as an integral part of the collimating optics. The assumption underlying this geometry is flawed and does not work for all x-ray generators. To correct this defect, an additional pinhole was designed and manufactured by Molecular Metrology, Inc., of Northampton, MA. The new pinhole, 200 μm in diameter, is located just downstream of the monochromator, well upstream of the second pinhole, as shown in Figure 4. The new pinhole is under vacuum, independently adjustable from outside the vacuum, and has a kinematic mount geometry. The SAXS camera now mimics the established geometry of two-pinhole camera design [17]. As illustrated in Figure 5, the spurious scatter around the beamstop has been eliminated. The ultimate resolution of the camera has been improved from 25 nm to ~45 nm, making the instrument well suited for most basic SAXS studies [18].

In addition to conventional SAXS data collection, in which the sample is held in a perpendicular orientation to the incident radiation, data was collected for the samples at a series of inclinations to the incident beam. To achieve this geometry, sample holders were physically bent to each of three angles—30°, 45°, and 60°. To perform measurements at 90°, each specimen was cut into strips, which were then affixed on edge to a 0°-tilt sample holder. In this way, five angles of tilt were achieved.

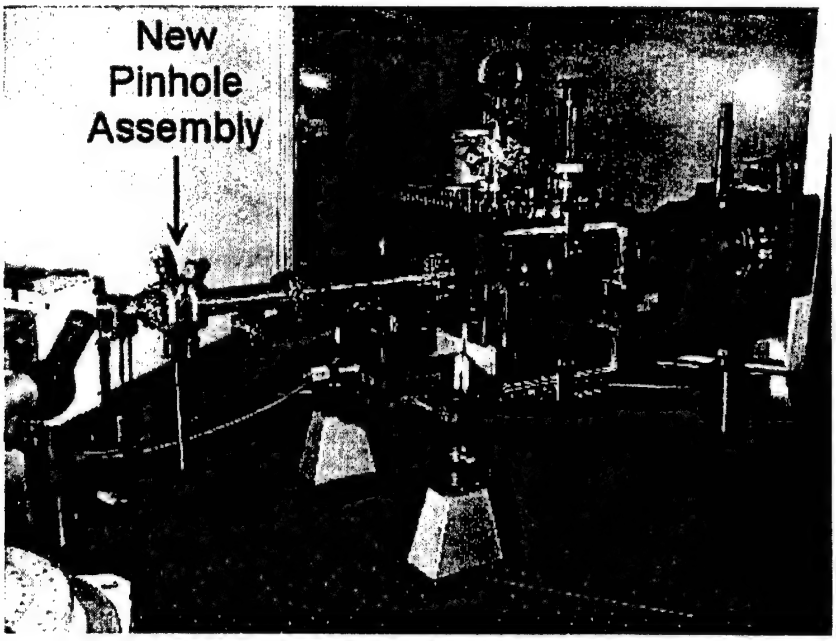

Figure 4. Picture of the SAXS camera, including the new 200-μm pinhole immediately downstream from the monochromator. The pinhole assembly is independently supported, under vacuum, and independently adjustable from outside the evacuated flight path.

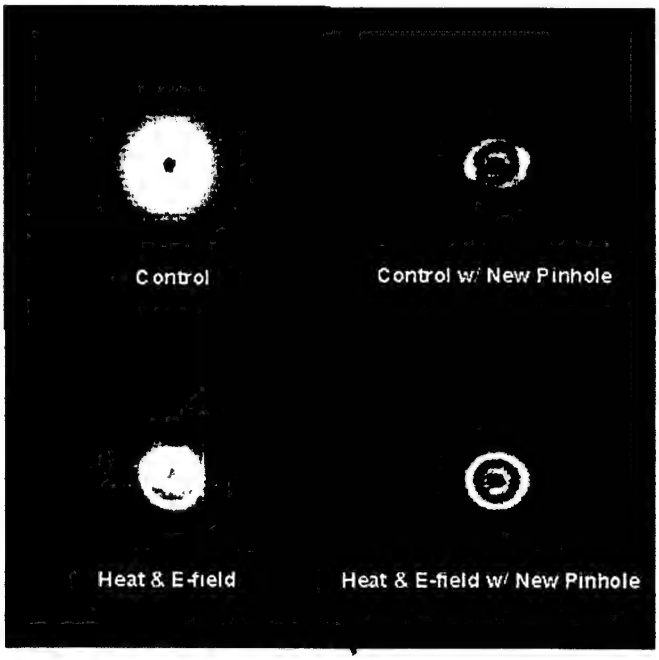

Figure 5. Schematic showing improvement in low-angle resolution with addition of second collimating pinhole. The improved collimation allows resolution of features up to 45 nm in length.

2.4.2 Transmission Electron Microscopy (TEM)

TEM was performed on representative SIBS samples. After embedding the samples in epoxy for better stability and handling during sectioning, ultrathin sections were collected using a Leica UCT ultramicrotome, operated at cryogenic temperatures, and a Diatome diamond knife. Section thickness was ~50 nm. The ultrathin sections were collected onto TEM grids and then exposed to RuO_4 vapor for 30 min. The vapor stain of RuO_4 provided enhanced mass-thickness contrast in TEM. TEM images were collected using a JEOL 100CX operated at 100-kV accelerating voltage.

3. Results and Discussion

3.1 TEM Results

Figure 6 shows representative TEM data from a sample which was heated and from a sample which was heated and subjected to an electric field. These images show that a cylindrical morphology is present in the samples. Unfortunately, the quality of the TEM data was not sufficient for a thorough assessment of the morphology in real space nor for a definitive conclusion on the effect of the poling process. The low image quality was due to difficulties in sample preparation. TEM required microtomed samples, which were challenging to prepare due to the rubbery nature and thinness of the SIBS films. Sample preparation was further complicated by the small samples sizes and deformed sample geometries produced by the annealing and poling processes. However, it is clear from Figure 6 that the general characteristics of a cylindrical morphology are present in both samples. Hexagonally arrayed microdomains are visible, corresponding to cylinders viewed end-on, as well as elongated microdomains, corresponding to cylinders viewed normal to the cylindrical axis.

3.2 SAXS Results

Figure 7 shows the circularly averaged intensity as a function of scattering angle for the poled, heated SIBS film. The film is normal to the incident x-ray beam. The identification of Bragg reflections at $q^*\sqrt{3}$, $q^*\sqrt{4}$, and $q^*\sqrt{7}$, where q^* is the scattering angle of the primary Bragg reflection, is correct for a morphology of hexagonally packed cylinders [19]. Combined with the TEM data from Figure 6, a positive identification of a cylindrical morphology in the bulk is certain.

Before presenting the results from the tilt angle SAXS measurements, it is useful to illustrate the expected scattering data for some representative morphologies.

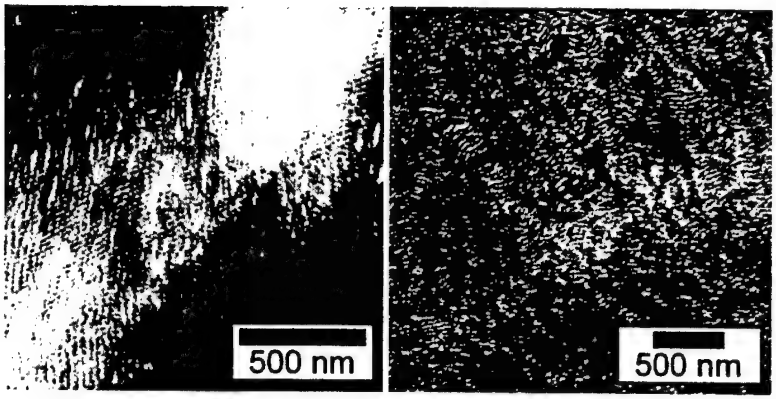

Figure 6. TEM micrographs from samples which are (a) heated but unpoled and (b) heated and poled using the electric field apparatus. While the images clearly show the difficulty experienced in preparing these samples for microscopy, the morphology observed appears to be cylindrical, in agreement with the previous work on this material and with the SAXS data collected from these samples.

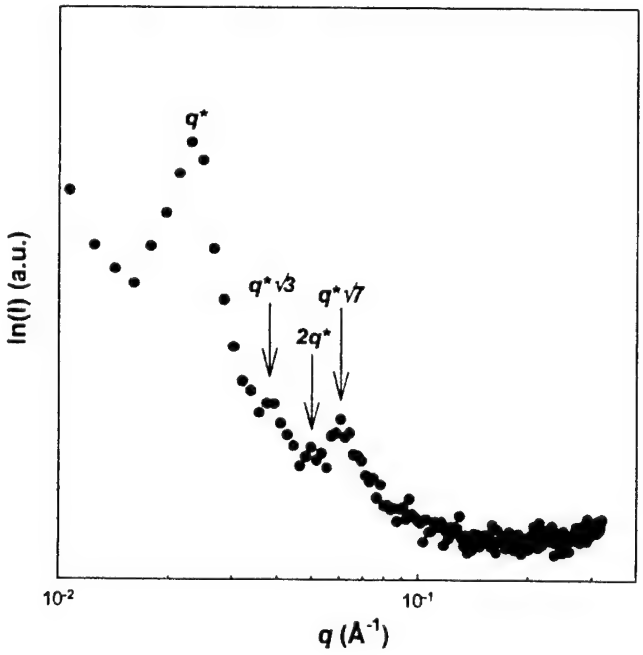

Figure 7. SAXS data from the heated and poled sample, taken at a $\phi = 0°$ tilt and circularly averaged. Bragg reflections at $\sqrt{3}$, 2, and $\sqrt{7}$ times the primary Bragg reflections identify the morphology as hexagonally packed cylinders.

In the simplest case, under equilibrium conditions and in the bulk, a multiple-grained morphology in which the cylinder axes are three-dimensionally, randomly oriented would occur. The patterns obtained for all tilts would be rings as all orientations of the morphology are present in every orientation. This is the most commonly observed type of SAXS pattern in block copolymer morphology studies and is well described by circularly averaged intensity data, as presented in Figure 7.

However, in this work, the goal was to create a non-equilibrium bulk morphology. Therefore, Figures 8 and 9 show illustrations of the different two-dimensional SAXS data that would be expected for several different possible variations of a cylindrical morphology. In Figure 8a, the SAXS data for a single domain of hexagonally packed cylinders oriented perpendicular to the plane of the film is shown. At $\phi = 0°$, six spots appear, reflecting the hexagonal packing of the cylinders. For all other tilt angles, only the reflections arising from the intercylinder distance are seen. In Figure 8b, the expected scattering data for a single grain in the plane of the film is illustrated. The scattering data should mirror that shown in Figure 8a, where the hexagonal symmetry is seen only when the incident radiation is aligned with the cylinder axis. For all other tilt angles, only two spots appear.

Figure 9 shows representations of the SAXS data expected for multiple grains of hexagonally packed cylinders. In Figure 9a, a sample with multiple grains of hexagonally packed cylinders, all oriented normal to the sample plane but with randomly oriented hexagonal lattice vectors, is tilted about an axis normal to the cylinders. In contrast to Figure 8a, the hexagonal symmetry here is lost at $\phi = 0°$ because all possible orientations of the hexagonal lattice unit vectors are present for cylinders normal to the film. In effect, the hexagonal array seen for $\phi = 0°$ in Figure 8a is present in all orientations. However, because all the cylinder axes are perfectly aligned normal to the plane of the film, at any tilt greater than $\phi = 0°$, only the two reflections for the intercylinder distance are detected.

Figure 9b shows the most interesting set of expected diffraction patterns for the cylindrical morphology. The domains are all oriented so that the cylinder axes lie within the plane of the film, while the individual grains are randomly oriented with respect to each other. The SAXS data show a marked transition from $\phi = 90°$ to $\phi = 0°$. At $\phi = 90°$, even though the different domains are present in all orientations, the hexagonal symmetry is observed because of the symmetry of the morphology in reciprocal space. As the tilt is decreased, the (0 1) reflections are lost, while the (11), (−1 −1), (10), and (−1 0) reflections draw closer to each other in a prescribed manner [5]. Finally, at $\phi = 0°$, the reflection arising from the intercylinder separation appears, but because all orientations of the cylinder axes within the plane of the film are present, the reflections form a ring.

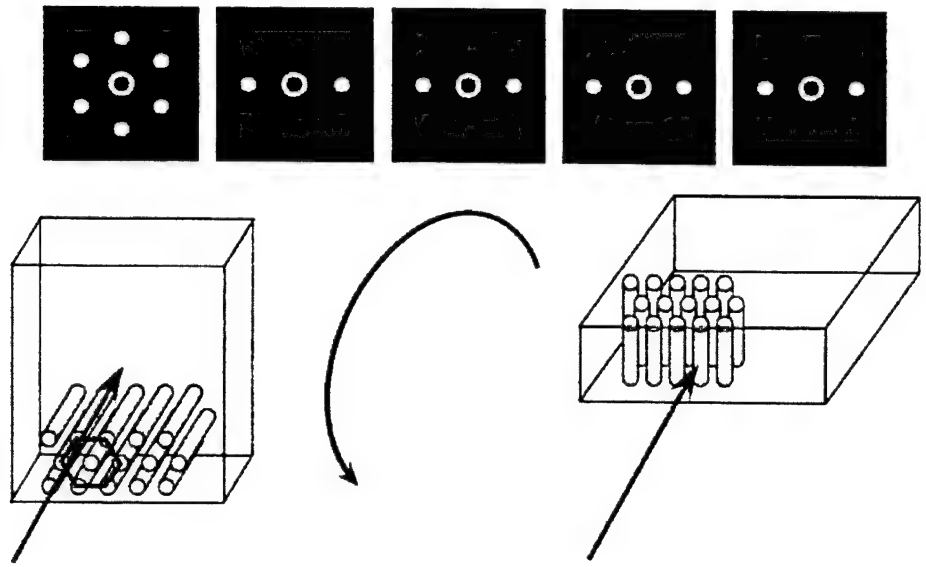

(a) Cylinders oriented normal to the film plane.

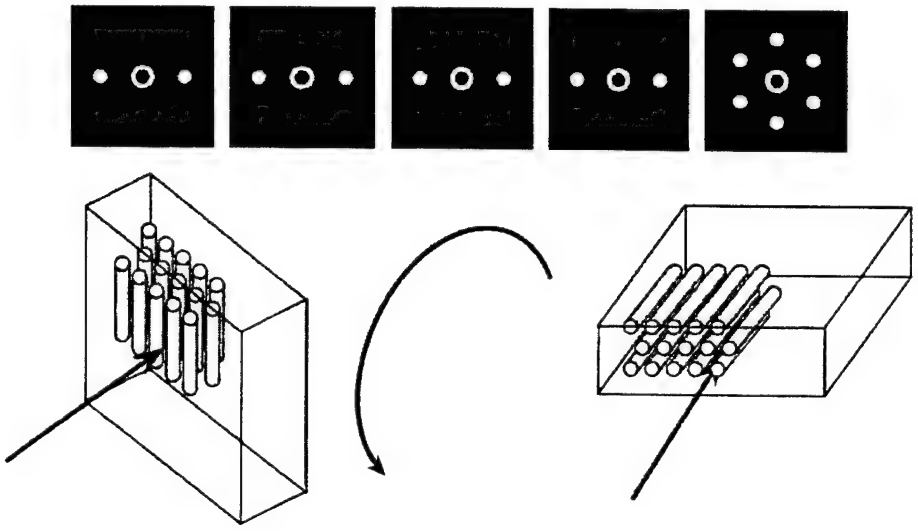

(b) Cylinders oriented in the film plane.

Figure 8. Schematics of the expected SAXS scattering patterns for single-grain structures as a function of tilt angle ϕ. The tilt angle increases from $\phi = 0°$ to $\phi = 90°$ from left to right.

Figure 10 shows the SAXS data collected for this experiment. As the sample is tilted, ϕ increases until it reaches 90°, at which point the x-ray beam is entering the edge of the sample and traveling in the plane of the film. A significant limitation of this experiment was that different sample holders were used for each tilt angle, requiring the samples to be remounted for each measurement.

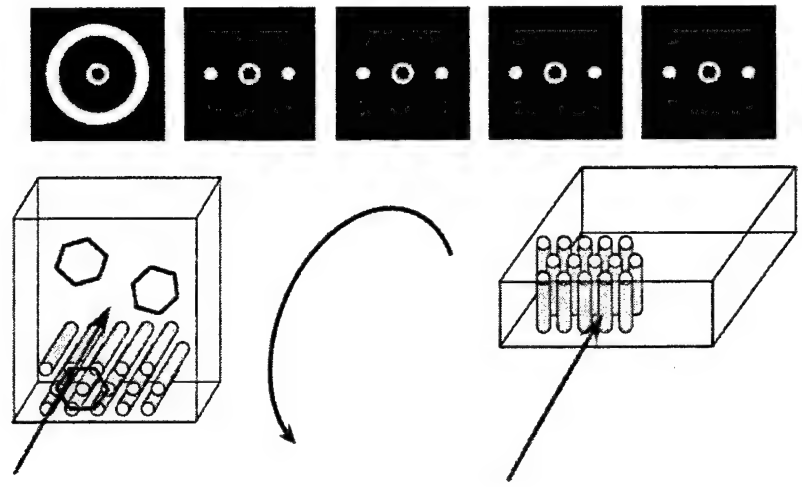

(a) Cylinders oriented normal to the film plane.

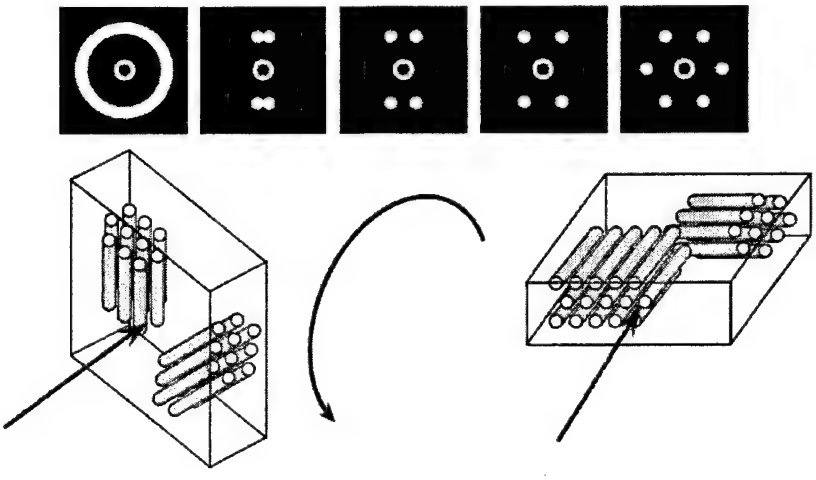

(b) Cylinders oriented in the film plane.

Figure 9. Schematics of the expected SAXS scattering patterns for granular structures as a function of tilt angle ϕ. The tilt angle increases from $\phi = 0°$ to $\phi = 90°$ from left to right.

Minor variations in sample rotational position were undoubtedly introduced during this process. In addition to these minor variations, it was possible that the samples were even flipped or fully rotated (in the sample plane) by 90° or 180°.

Figure 10a shows the SAXS data collected for the unheated and unpoled sample. For $\phi = 0°$-45°, arcs are seen. At $\phi = 60°$ and 90°, the arcs appear wider. The general appearance of two peaks at low angles is consistent with a cylindrical in-plane morphology. The fact that the peaks are arcs rather than spots indicates

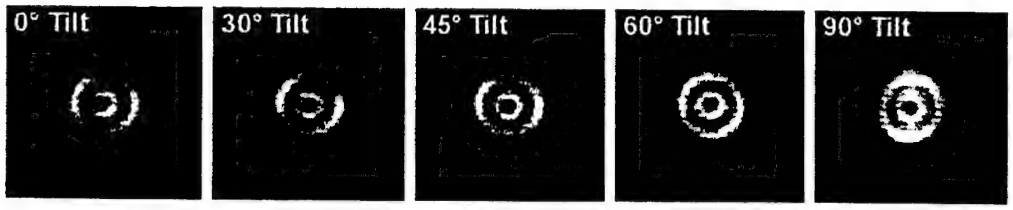

(a) Tilt series for unheated, unpoled sample.

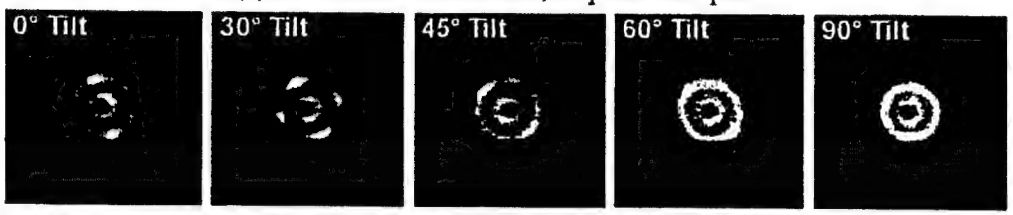

(b) Tilt series for heated, but unpoled sample.

(c) Tilt series for heated, poled sample.

Figure 10. SAXS data collected at tilt angles for each condition: (a) unheated and unpoled, (b) heated and unpoled, and (c) heated and poled.

that there is some variation in the in-plane alignment of the cylinder axes. The appearance of a more uniform ring at higher angles is consistent with the presence of more cylinders viewed end-on, which would also be expected for the case of a random in-plane cylindrical microstructure.

Figure 10b shows the SAXS data collected for the heated and unpoled sample. At $\phi = 0°$, two sharp, strong peaks are clearly evident. At $\phi = 30°$, the two strong peaks remain, accompanied by two weaker but similarly sharp peaks. At $\phi = 45°$ and $\phi = 60°$, two slightly broader peaks are observed. At $\phi = 90°$, a more circular diffraction pattern emerges, with very little circular variation for the $\phi = 90°$ case. This data clearly indicates the presence of an in-plane cylindrical morphology. The sharpness of the peaks indicates a high degree of long-range order. The only anomalous data is the appearance of the two weaker peaks at $\phi = 30°$. In this case, given the other data, it is likely that the x-ray beam is intersecting a second, large and well-ordered grain of cylinders in the plane of the film. The better ordering in this sample, compared with the unheated and unpoled sample, is not surprising. It is well known that annealing a microphase separated block copolymer sample will allow the self-assembly process to proceed toward equilibrium and remove kinetic entrapment features that tend to blur the

Figure 10c shows the SAXS data collected for the heated and poled sample. At low angles, wide arcs are seen. At $\phi = 60°$, very little scattering is observed. At $\phi = 90°$, a circular pattern is measured, along with a vertical scattering band. This vertical band is most likely an artifact, probably introduced by the presence of supporting Kapton film layers above and below the sample. The low intensity at $\phi = 60°$ is surprising and may indicate that a smaller portion of the sample was exposed to the incident beam.

In general, the SAXS results for the heated and poled sample seem to indicate a random in-plane cylindrical morphology. The presence of arcs at low angles rather than uniform rings indicates that there is some in-plane orientational bias to the morphology. This bias would not be present for a morphology of cylinders oriented normal to the film plane. The uniform ring at $\phi = 90°$ is also consistent with a random in-plane morphology.

An alternative interpretation of the heated and poled sample is also possible. The TEM data showed that vastly different morphological orientations can exist within a granular structure. If the sample contained some grains with a cylindrical morphology oriented in the film plane, while other grains had a cylindrical morphology oriented normal to the film plane, then a less straightforward SAXS profile would result. At $\phi = 0°$, we speculate that such a granular structure would produce a scattering pattern intermediate between well-ordered in-plane domains (small arcs) and domains oriented normal to the film plane (circular pattern). The data at $\phi = 0°$ for the heated and poled sample may be consistent with this result. For this granular structure, we would expect to see some peaks at $\phi = 90°$ due to the presence of the microstructure oriented normal to the film plane. Such peaks are not clearly evident in the measured pattern. However, the relative strengths of the scattering patterns for each microstructure feature are not clear. Therefore, it is difficult to predict what the precise averaged scattering pattern would be for these complicated granular structures. At best, we can say with certainty that a majority of the grains for the heated and poled sample are not oriented normal to the film plane.

4. Conclusions

The SAXS data provides no firm evidence that electrostatic melt processing is causing the SIBS film to orient along the electric field lines, normal to the film plane. The data seems to indicate that the microstructure for the samples is predominantly oriented in the film plane. However, it is also clear that the morphology is different for the heated and unpoled sample as compared with the heated and poled sample. Since the only difference between the samples is the application of an electric field, these results seem to indicate that the electric

field is having some effect on the microstructure. One possibility is that the presence of the electric field somehow impedes the formation of long-range order during annealing, although such an effect has never been documented before.

Another possibility is that the microstructure is not fully aligned but is in some intermediate state. In section 3.2, one possibility, a multigrained structure consisting of both in-plane and out-of-plane microstructures, was proposed. Other possibilities exist. If the microstructure was undergoing a domain flow or rotation reorientation mechanism, it is possible that some of the grains possessed some sort of deformed morphology. The physics of phase separation in block copolymers prevent deformation of the cylindrical domains into oblate ellipsoids (as appears in the schematic in Figure 1b). However, curved or kinked cylindrical domains are possible. The cylinders could also still be straight, but aligned at some intermediate tilt angle between in-plane and out-of-plane. Such a progression was observed for a lamellar microstructure by Amundson et al. [9]. The scattering patterns for such complex morphologies are difficult to predict and sometimes not unique, so it is difficult to rule out such microstructures.

The fact that the block copolymer microstructure has not been completely aligned normal to the film plane by our processing is not entirely surprising. Previous researchers have found that, whether using domain flow reorientation or domain dissolution, up to 24 hr of electrostatic melt processing is often required to produce full reorientation [8, 9]. In these cases, the dielectric contrast of the phases was significantly higher than that of the PS and PIB phases in our SIBS film. Therefore, our material could, in fact, require even more time to fully align.

The inability of our setup to pole films for more than 1 hr is a key limitation of these experiments. Many electrode and sample geometries were tried, but clearly a satisfactory arrangement was not achieved. It is unclear why dielectric breakdown and short circuiting were so difficult to eliminate in our poling stack, as other researchers have achieved much better processing performance.

Another shortcoming of the current results is the lack of good TEM images for the processed SIBS samples. The SAXS measurements provide some information, but the potential complications introduced by intermediate morphologies and granular structures prevent conclusive interpretation. A combination of thorough TEM analysis with SAXS data is necessary to provide unambiguous characterization of the block copolymer morphology.

5. References

1. Crawford, D. M., E. Napadensky, N. Beck Tan, J. Sloan, D. A. Reuschle, D. A. Mountz, K. A. Mauritz, K. S. Laverdure, S. P. Gido, W. Liu, and B. Hsiao. "Semipermeable Membrane From Ionomeric Self-Assembling Block Copolymer." ARL-TR-2403, U.S. Army Research Laboratory, Aberdeen Proving Ground, MD 2001.

2. Napadensky, E., D. Crawford, J. Sloan, and N. Beck Tan. "Viscoelastic and Transport Properties of Sulfonated PS-PIB-PS Block Copolymers." ARL-TR-2482, U.S. Army Research Laboratory, Aberdeen Proving Ground, MD 2001.

3. Amundson, K., E. Helfand, X. Quan, and S. D. Smith. "Alignment of Lamellar Block Copolymer Microstructure in an Electric Field. 1. Alignment Kinetics." *Macromolecules,* vol. 26, pp. 2698–2703, 1993.

4. Thurn-Albrecht, T., R. Steiner, J. DeRouchey, C. M. Stafford, E. Huang, M. Bal, M. Tuominen, C. J. Hawker, and T. P. Russell. "Nanoscopic Templates From Oriented Block Copolymer Films." *Advanced Materials,* vol. 12, no. 11, pp. 787–791, 2000.

5. Thurn-Albrecht, T., J. DeRouchey, T. P. Russel, and H. M. Jaeger. "Overcoming Interfacial Interactions With Electric Fields." *Macromolecules,* vol. 33, no. 9, pp. 3250–3253, 2000.

6. Thurn-Albrecht, T., J. Schotter, G. A. Kastle, N. Emley, T. Shibauchi, L. Krusin-Elbaum, K. Guarini, C. T. Black, M. T. Tuominen, and T. P. Russell. "Ultrahigh-Density Nanowire Arrays Grown in Self-Assembled Diblock Copolymer Templates." *Science,* vol. 290, pp. 2126–2129, 2000.

7. Mansky, P., J. DeRouchey, T. P. Russell, J. Mays, M. Pitsikalis, T. Morkved, and H. Jaeger. "Large-Area Domain Alignment in Block Copolymer Thin Films Using Electric Fields." *Macromolecules,* vol. 31, pp. 4399–4401, 1998.

8. Morkved, T. L., M. Lu, A. M. Urbas, E. E. Ehrichs, H. M. Jaeger, P. Mansky, and T. P. Russell. "Local Control of Microdomain Orientation in Diblock Copolymer Thin Films With Electric Fields." *Science,* vol. 273, pp. 931–933, 1996.

9. Amundson, K., E. Helfand, D. D. Davis, X. Quan, and S. S. Patel. "Effect of an Electric Field on Block Copolymer Microstructure." *Macromolecules,* vol. 24, pp. 6546–6548, 1991.

10. Strand, S. R., and S. Kim. "Dynamics and Rheology of a Dilute Suspension of Dipolar Nonspherical Particles in an External Field: Part 1. Steady Shear Flows." *Rheologica Acta,* vol. 31, pp. 94–117, 1992.

11. Okagawa, A., R. G. Cox, and S. G. Mason. "Particle Behavior in Shear and Electric Fields VI: The Microrheology of Rigid Suspensions." *Journal of Colloid and Interface Science,* vol. 47, no. 2, pp. 536–567, 1974.

12. Vyakarnam, M. N., and L. T. Drzal. "Novel Processing and Performance of Aligned Discontinuous Fiber Polymer Composites." *Proceedings of the Society for Plastics Engineers ANTEC,* pp. 2531–2535, 1996.

13. Itoh, T., S. Masuda, and F. Gomi. "Electrostatic Orientation of Ceramic Short Fibers in Liquid." *Journal of Electrostatics,* vol. 32, pp. 71–89, 1994.

14. Saville, D. A. "Electrohydrodynamics: The Taylor-Melcher Leaky Dielectric Model." *Annual Review of Fluid Mechanics,* vol. 29, pp. 27–64, 1997.

15. Torza, S., R. G. Cox, and S. G. Mason. "Electrohydrodynamic Deformation and Burst of Liquid Drops." *Philosophical Transactions of the Royal Society of London, Series A: Mathematical and Physical Sciences,* vol. 269, pp. 295–319, 1971.

16. Tse, M. F., H. C. Wang, T. D. Shaffer, K. O. McElrath, R. Krishnamoorti, and M. Modi. "Physical Properties of Isobutylene-Based Block Copolymers." Proceedings of the Rubber Division, American Chemical Society, Cleveland, OH, 21–24 October 1997.

17. Rieker, T. P., and P. F. Hubbard. *Review of Scientific Instruments.* Vol. 69, p. 3504, 1998.

18. Mildner, D. F. R., and J. M. Carpenter. *Journal of Applied Crystallography.* Vol. 17, p. 249, 1984.

19. Cullity, B. D. *Elements of X-ray Diffraction, 2nd ed.* Reading, MA: Addison-Wesley, 1978.

REPORT DOCUMENTATION PAGE

Form Approved
OMB No. 0704-0188

1. AGENCY USE ONLY *(Leave blank)*	2. REPORT DATE	3. REPORT TYPE AND DATES COVERED
	August 2002	Final, October 2000–October 2001

4. TITLE AND SUBTITLE
Self-Assembling Nanomembranes Through Electrostatic Melt Processing of Copolymer Films

5. FUNDING NUMBERS
DRI-FY01-WM

6. AUTHOR(S)
Eric D. Wetzel and Frederick L. Beyer

7. PERFORMING ORGANIZATION NAME(S) AND ADDRESS(ES)
U.S. Army Research Laboratory
ATTN: AMSRL-WM-MB
Aberdeen Proving Ground, MD 21005-5069

8. PERFORMING ORGANIZATION REPORT NUMBER
ARL-TR-2800

9. SPONSORING/MONITORING AGENCY NAMES(S) AND ADDRESS(ES)

10.SPONSORING/MONITORING AGENCY REPORT NUMBER

11. SUPPLEMENTARY NOTES

12a. DISTRIBUTION/AVAILABILITY STATEMENT
Approved for public release; distribution is unlimited.

12b. DISTRIBUTION CODE

13. ABSTRACT*(Maximum 200 words)*

Polystyrene-polyisobutylene-polystyrene (SIBS) block copolymer films have been electrostatically melt processed in order to induce a preferential orientation in the material microstructure. The results show that electrostatic melt processing is inducing some change in the microstructure, but full reorientation is not being achieved. The low dielectric contrast of the SIBS blocks as well as the relatively short electrostatic processing times are the likely causes of incomplete alignment.

14. SUBJECT TERMS
copolymer, SIBS, polystyrene, polyisobutylene, barrier material, chem-bio, electrostatic, electric field

15. NUMBER OF PAGES
27

16. PRICE CODE

17. SECURITY CLASSIFICATION OF REPORT	18. SECURITY CLASSIFICATION OF THIS PAGE	19. SECURITY CLASSIFICATION OF ABSTRACT	20. LIMITATION OF ABSTRACT
UNCLASSIFIED	UNCLASSIFIED	UNCLASSIFIED	UL

INTENTIONALLY LEFT BLANK.